Materials Research. 2022; 25:e20210485
DOI: https://doi.org/10.1590/1980-5373-MR-2021-0485

Metallurgical Processing for Impregnated Thermionic Cathodes Manufacturing

Glauco P. Zanella[a], Gabriel G. J. de Sousa[a], Cláudio C. Motta[a]*

[a]*Universidade de São Paulo, São Paulo, SP, Brasil.*

Received: September 22, 2021; Revised: December 20, 2021; Accepted: January 13, 2022.

A metallurgical process using a very high temperature Mo-Ru brazing filler alloy to join a controlled porous tungsten cathode button and a single-crystalline molybdenum cathode body for microwave tubes manufacture was developed[†]. The Mo-Ru brazing alloy was obtained by mixing and milling powders in the eutectic composition with a binder, and a braze paste was applied on the surface cathode parts. Brazing was performed in two temperatures by using a resistive dry hydrogen cold wall furnace for 10 minutes: at 1890 °C and 1967 °C. It was observed a fillability by the Mo-Ru system only in the tests performed in temperatures above 1967°C. The brazed samples were analyzed by Scanning Electron Microscopy coupled to Energy Dispersive Spectroscopy. It was observed absence of microstructural defects in the interface between the tungsten porous and dense molybdenum joint. Stress-strain tests, followed by SEM analysis were performed to determine the mechanical behavior of the brazing joining. The results indicate the origin region of the cracking and show an intergranular propagation; some evidence as grain cleavage indicates a brittle failure behavior.

Keywords: *powder metallurgy, Mo-Ru brazing alloy, impregnated thermionic cathode processing.*

1. Introduction

Barium aluminate impregnated or dispenser thermionic cathodes are components responsible for electron emission long-life properties of electron guns in power and high power microwave devices such as traveling wave tubes (TWTs) and klystrons amplifiers. Moreover, as the electron beam is the energy source for microwave tubes, the microwave output power will always be some fraction of the total beam power. The electron beam is an essential component of all vacuum electronics devices from which the microwave power is extracted. In other words, vacuum microwaves devices are energy converters, where the kinetic energy from the electron beam is converted into microwave energy[1].

The principle of working of impregnated thermionic cathodes is well established and discussed in some microwave tube textbooks[2,3]. It is based on the thermionic emission of electrons from the surface metal to vacuum when metal is to heat above 1100 °C[4]. Despite the electron emission control of impregnated thermionic cathodes being based on quantum mechanics principles, the construction of the thermionic cathodes for a long lifetime and reliably operation of microwave tubes is related to, mainly, the material and metallurgical processing[5,6].

During the processing of thermionic cathodes, a fundamental step is to join the porous tungsten matrix to the molybdenum cathode body. This is commonly made by the thermally activated process of brazing. In this technique, a second material, that has a melting point below both the parts, like a filler or a brazing alloy, is put near the joint. Then, the parts are heated to a temperature high enough to melt the filler but not the parts. This way, the molten filler metal spreads into the joint by the capillary attraction, and then when the parts are cooled to freeze between the filler metal, a chemical interaction between the surfaces and the filler occurs, promoting an atomic bonding and anchoring the parts together[7,8].

When it comes to the thermionic cathodes, the filler must have a good wettability to both the tungsten and the molybdenum; besides that, it must have a higher melting point than the common operation temperature of thermionic cathodes, which is typically 1200°C. Further considerations to this process are thermal shock followed by crack propagation, re-melting of the filler material, contamination, and matrix insulation from electron emission promoted by the filler. In addition, the melting point of the filler must be achieved by the furnace used in the processing.

Some good results could be achieved using the Ni-Mo system in the eutectic composition (38.8 at. % of molybdenum), which melts around 1310 °C[9]. However, when applied to type B cathode, the Ni-Mo system implies a re-melting in the impregnation step of the barium calcium aluminate 5:3:2, which has a melting point above 1600°C. This situation can be overcome using the Mo-Ru brazing alloy, which the eutectic point is around 1955°C, as can be seen at the Mo-Ru phase diagram at 42.9 wt. % of ruthenium point[10,11].

The present work aims to report a brazing process developed to join a porous tungsten cathode button to a dense molybdenum cathode body using a eutectic Mo-Ru brazing paste as filler and a dry hydrogen resistive furnace. It is also presented a new route to a porous tungsten matrix production and some improvements achieved since previous works on the inductive heating system to matrix decopperization[12].

*e-mail: ccmotta@usp.br

[†]Patent pending: BR 1020190118628

2. Experimental Procedure

The metallurgical processing for thermionic cathode manufacturing developed will be described as followed: cathode button manufacture, metal filler preparation, and cathode brazing processing.

2.1. Cathode button processing

2.1.1. Cathode button preparation

The cathode button was obtained from a mixture of copper (Cu) and tungsten (W) powders. The powders, with a nominal average particle size between 20 and 75 μm, were weighed and mixed using an Agatha mortar for 15 minutes. The Cu/W ratio was empirically determined based on the specified cathode density, closely to 30% in volume of pores. The ratio allowed to obtain the best results was W-20wt%Cu, as published in a previous work[12].

After homogenization, the mixture was pressed in a stainless-steel cylindrical matrix, with a hard metal ending punch, in a uniaxial hydraulic press (MARCOM, MPH-30) under 416 MPa, Figure 1. The internal diameter of the press matrix was about 10.25 mm. This dimension was determined based on the densification of the final diameter of the button. As this button was lathe machined and heated, the expected diameter dimension of 9 mm was achieved at the final step.

Following the pressing step, the button went to the pre-sintering process. This process consists in heating the button at a temperature over the copper melting point (approximately 1200°C) in an induction heated furnace with a reductive atmosphere of hydrogen with 99.999% purity, - 60°C of dew point, and 3 l/min gas flow for 5 minutes. Thus, the copper melts and works as a filler among the tungsten particles, adding mechanical resistance to the button.

The experimental apparatus for this step consisted of a molybdenum crucible held inside in a quartz tube involved by a 3 inches coil with four turns, as shown in Figure 2. An induction power supply, with an automatic impedance matching control, was used for heating (Ambrell, Easyheat model 3542).

The eddy currents generated within the crucible due to electromagnetic induction leads to Joule heating of the system. The temperature ramp, necessary to prevent cracking generation, was controlled by the electric current in the coil (from 205.8 A to 333.9 A at 8.4 A/min rate). During the heating process, the crucible temperature was measured using a DFP 2000 optical pyrometer. The process parameters for this step are shown in Table 1. The molybdenum crucible

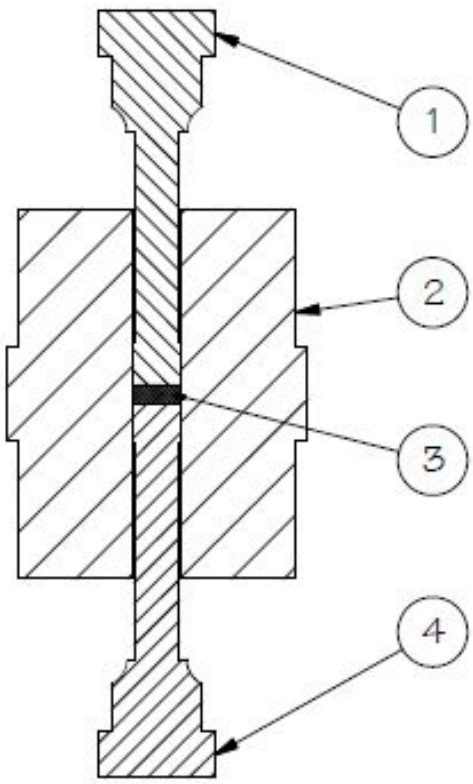

Figure 1. Pressing matrix: (1) top die punch; (2) die; (3) cathode button; and (4) bottom die punch.

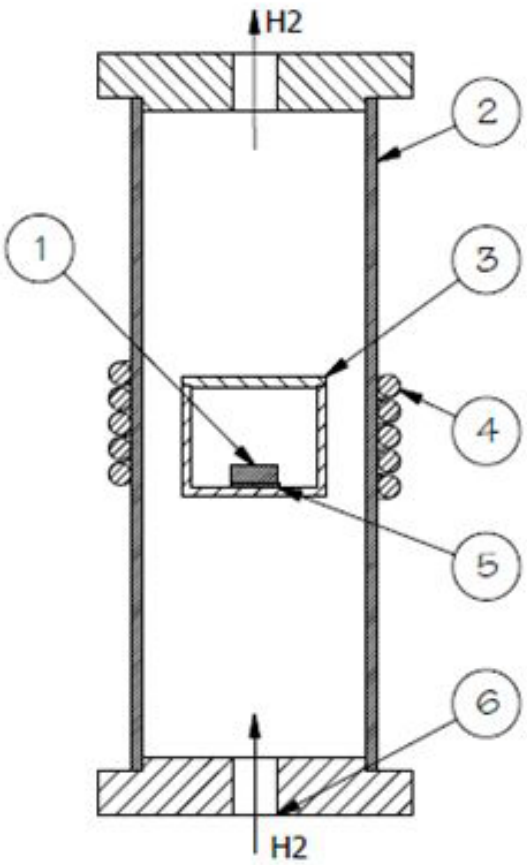

Figure 2. Induction heating jig for pre-sintering and decopperization steps: (1) cathode button; (2) quartz tube; (3) molybdenum crucible; (4) 3-inch coil with four turns; (5) alumina disk; and (6) dry hydrogen entrance.

has the capacity to process up to nine cathodes spaced by high alumina disks.

After the pre-sinter process, the cathode button was lathe machined. The curvature radius in the top face, necessary to the electron beam focusing, and the groove in the rear face were machined using a CNC lathe (ROMI, model Centur 30D). All the cathode dimensions were measured using a coordinate measuring machine (Mitutoyo, model M-7106) to ensure dimensional process control.

2.1.2. Decopperization

After machining, the composite W-20%Cu was submitted to a second heating to remove copper in a reducing atmosphere (H_2), named physical decopperization. In this step, the same previous apparatus was used to heat the composite with the same heating ramp of 8.4 A/min. The improved induction parameters to the decopperization step are shown in Table 2. These parameters allow the samples to achieve a temperature of 1600°C and stay there with a stable operation during a 6-hour process. At this temperature, copper evaporates from the structure and the porous tungsten cathode button is formed.

After the physical decopperization, a chemical etching was done to remove any residual copper not only from the surface but also from the tungsten matrix bulk. The etchant consists of immersing the tungsten matrix in a solution of nitric acid (50%vol.) in deionized water for 12 hours. After etching, the button was dipped in distilled water and ultrasonically cleaned to stop the etching process.

2.2. Metal filler preparation

2.2.1. Brazing alloy preparation

Based on the results obtained by joining single-crystalline molybdenum blocks (Hiraoka, 1992)[10], the goal was to join a tungsten porous matrix to a poly-crystalline molybdenum cathode body. Hiraoka mentioned that a Mo-40%Ru alloy powder of about 200 mesh was mixed with an organic solvent to spread into the joint in his paper. As Mo-Ru brazing alloy is not commercially available, it was also necessary to develop a route based on the principles of solid-state reaction[13].

The mixture composition was based on the Mo-Ru phase diagram. The eutectic composition can be found in the Mo-42.9 wt%Ru[11], different from the composition used by Hiraoka. The molybdenum and ruthenium powders (99.9% purity) with a nominal average particle size of 44 µm were weighed, mixed, and milled using a mortar for 30 minutes. At the final of the milling step, a homogeneous mixture was achieved.

Table 1. Parameters for the tungsten cathode matrix pre-sintering step.

Parameter	
Maximum coil current	333.9 A
Induction power	1900-2000 W
Maximum temperature	1200 °C
Heating and cooling times	60 min (total)
Plateau time	5 min
Heating chamber pressure	760 Torr
Hydrogen dry flow (H_2)	3 l/min

Table 2. Improved parameters for the tungsten cathode matrix decopperization step.

Parameter	
Maximum coil current	478.8 A
Induction power	3980 - 4040 W
Maximum temperature	1620 °C
Heating and cooling times	60 min (total)
Plateau time	6 h
Heating chamber pressure	760 Torr
Hydrogen dry flow (H_2)	3 l/min

2.2.2. Brazing paste preparation

In order to prepare the brazing paste a binder composed of isobutyl acetate, nitrocellulose (with a kinematic viscosity of 360 saybolt universal seconds), diethyl oxalate, and anhydrous ethyl alcohol was used following the route shown in Figure 3, with a defined ratio for each reagent of 28:1:5:10, respectively. The metallic powders of the Mo-Ru eutectic alloy were then added in stoichiometric quantities to produce a brazing paste with 70% by weight of solids. The paste brazing was stirred using a glass rod for homogenization, spread into the cathode parts using a brush, and finally vacuum dried for 2 hours.

2.3. Cathode brazing processing

Figure 4 shows the points where the brazing paste was spread to promote the union of the cathode parts. A layer of paste was spread into the contact face in both components, and then another layer was spread into the rear face. This step is especially needed to seal the tungsten button rear surface and avoid any thermionic emission in the heater direction.

The brazing was done using a special all Mo fixture assembled in the heating system shown in Figure 5, put inside of a very high temperature (2000 °C), cold wall furnace (CAMCo, Model G-2000) and a 3.3 l/min hydrogen flow, with a - 60°C of dew point, kept a reducing atmosphere. The temperature of the chamber was measured by a thermocouple (type C) located inside the heating chamber. Two temperature levels were used in different tests: 1890 °C and 1967 °C; in both experiments, the levels were maintained for 5 minutes aiming to melt the brazing alloy.

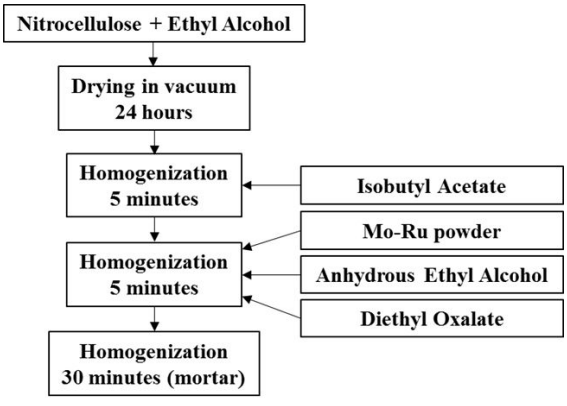

Figure 3. Flowchart for the Mo-Ru brazing paste.

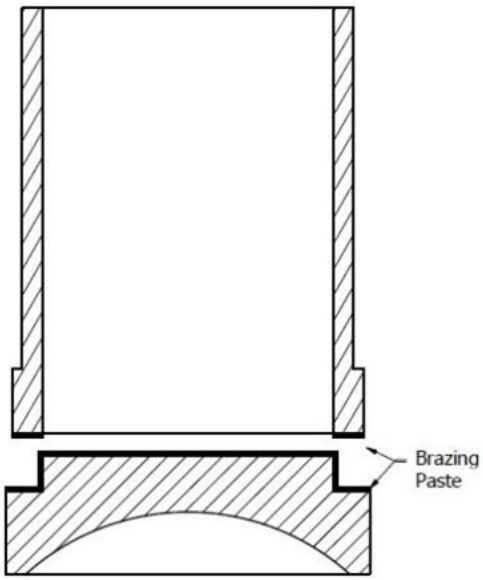

Figure 4. Schematic drawing for the brazing paste application.

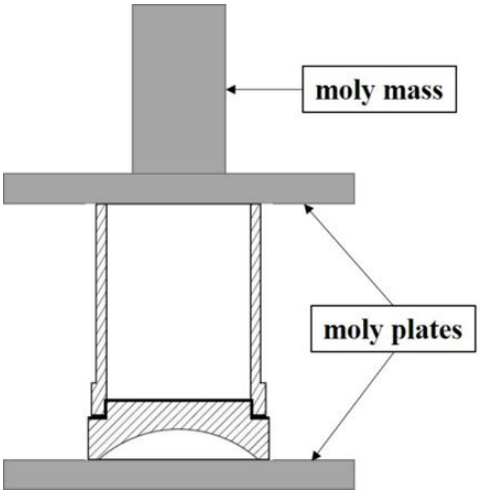

Figure 5. Schematic jig drawing for hydrogen brazing process.

2.4. Structural and compositional analyses

Considering that the initial composition of the matrix samples is W-20wt%Cu and the mass loss during the decopperization process is basically related to copper loss, it is possible to infer the momentaneous composition based on the mass loss. This way, the samples were weighed after pre-sintering, physical decopperization, chemical etching, and final heating steps. Additionally, to check that the mass loss observed along the process was related to copper indeed, an Energy Dispersive X-rays Fluorescence (EDX) analysis was made after chemical etching.

The porosity and the relative density were calculated according to the ASTM C20-00(2015)[14]. The dried mass, immersed mass, and wet mass were measured in an analytical balance (GEHAKA, model AG-200) with an arrangement to weigh using the Archimedes' method.

2.5. Microstructural analysis

To better investigate the brazed junction behavior two microstructural analyses were made, Optical Microscopy (ZEISS, Axio Image M2m) and Scanning Electron Microscopy (SEM), (JEOL 6460LV) by using secondary electrons and backscattered electrons modes.

The samples were prepared, by a longitudinal dimension cutting in the middle of the matrix diameter to observe the junction in the two edges, cut using a wire cut electric discharge machine (Agie Charmilles, Cut 20 P), and manually polished with a 1 μm diamond paste.

Three samples were analyzed by using the optical microscope. The junction, porosity, and sealing were analyzed by this technique. Amplifications from 25x to 100x were used to characterize the samples; at least three regions per sample were considered in the analysis. As it was not possible to note high contrast between the alloy and the cathode body region, SEM was used to observe atomic diffusion between the alloy and the parts using the Electron Dispersive Spectroscopy (EDS) module. Furthermore, a map was made considering W, Mo, and Ru to observe the distribution of the compounds in the junction region. The SEM analysis was made also considering three regions of the sample: the cathode body, the cathode button, and the brazing region.

2.6. Mechanical strength analysis

After the brazing step, it was necessary to qualify the formed junction. As the goal was to qualify especially the cathode joint in its characteristic dimensions, a jig was developed to test the sample in a strength test machine. As it can be seen in Figure 6, the strength test jig is composed of a clamp that is used to hold the cathode body sample and by a bottom punch that is used to transfer the tensile to the porous matrix button.

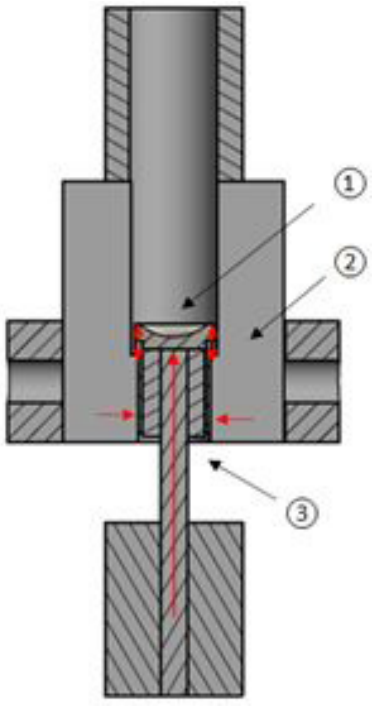

Figure 6. Arrangement to the strength test: 1 - cathode sample; 2 - clamp; and 3 - bottom punch.

The brazed cathode set was submitted to a tensile strength in a certified universal testing machine (Instron, model 1331). The displacement speed was 0.5 mm/min in room temperature. As the sample is held by the body and a force is applied through the bottom punch, a tension is formed on the region of the joint. After the strength test, the cracked sections were submitted to a SEM analysis, (JEOL 6460LV) aiming to obtain a better explanation of the cracking propagation and identify the origin region.

3. Results and Discussion

3.1. Compositional analysis

A cumulate mass loss plot of all the manufacturing steps, considering 12 samples, can be seen in Figure 7. After the physical decopperization process, it was noticed a mass loss between 8 and 15% in the samples. Based on the temperature the samples were submitted this mass difference refers to copper that was removed from them. It is relevant to notice that the copper is removed from the core of the samples and a little amount of that can remain on its contact surfaces with high alumina spaced disks. This way, an EDX analysis would confirm only the superficial amount of copper but not the actual average amount of the sample.

It was observed that the chemical etching in a solution of nitric acid (50% vol. in deionized water) was able to remove the residual copper as well to open the superficial pores[12]. Considering that the used solution is selective, the tungsten structure remains uninjured after the dipping process. After this process, both results indicated the lasting 5% of copper was removed. The mass difference between the initial and final samples was 20.0 ± 0.1% that was approximately the amount of copper within the initial mixture.

The EDX analysis made after the chemical etching confirmed that the mass loss was due to copper. The results can be seen in Table 3. In all EDX analyses, the residual copper was no more than 0.06 at. %, the results include the samples cut and analyzed in their cores.

3.2. Practical improvements

A processing improvement was obtained by changing the graphite crucible used to heat the samples for a molybdenum one[9,12]. A general design of the new crucible can be seen in Figure 8. The Mo crucible allows one to produce a porous tungsten matrix free from carbon contamination which implies a more reliable process of brazing, eliminating any contamination during processing, preserving the electron emission material purity, and increasing of cathode lifetime.

Furthermore, some practical advances were obtained by using the new route. The main improvement was to achieve a temperature of 1600°C without using any magnetic susceptor. The molybdenum crucible provided a better coupling with the magnetic field produced by the coil.

Moreover, the design of the crucible, that predicts a cover, makes it behave like a thermal reservoir based on the blackbody radiation effect. This guarantees a high thermal homogeneity and high thermal stability all along the process

Table 3. Chemical composition of cathode pellet after chemical etching obtained by an EDX analysis.

Sample	W (± 0.01 mol %)	Cu (± 0.01 mol %)	Others (± 0.01 mol %)
1	98.64	0.05	< 1.31
2	98.48	0.06	< 1.46
3	98.44	0.07	< 1.49
4	98.49	0.10	< 1.40
5	98.17	0.17	< 1.66
6	98.92	0.07	< 1.01
7	98.39	0.08	< 1.53
8	99.29	0.05	< 0.66
9	98.53	0.05	< 1.43
10	96.73	0.06	< 3.20
11	97.68	0.06	< 2.26
12	99.39	0.04	<0.57
Average	98.43	0.07	

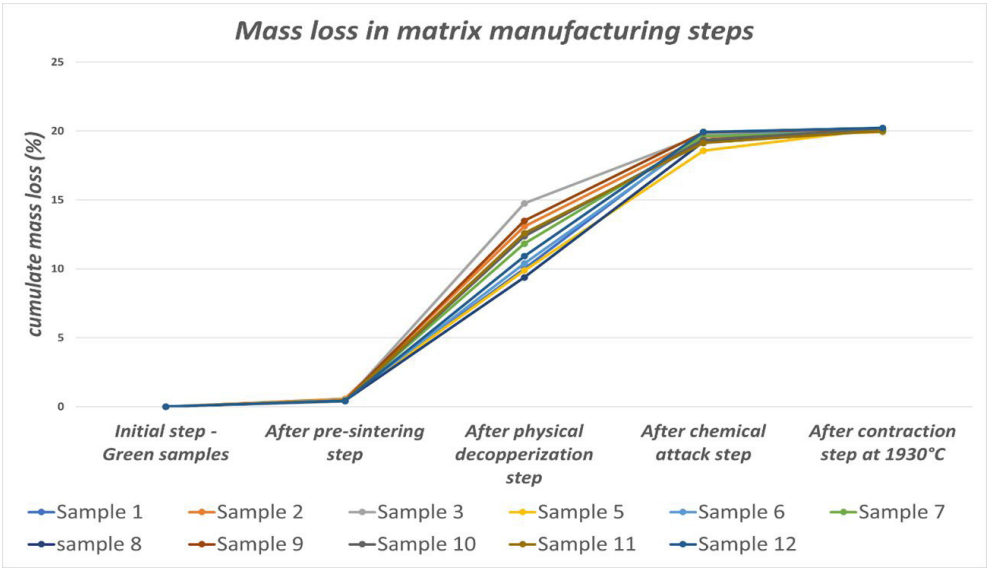

Figure 7. Cumulate mass losses along matrix manufacturing process.

Figure 8. Arrangement of the sample holder with the cathode buttons.

and allows one to process up to 9 cathodes button at the same time, limited only by the inner crucible volume.

Additionally, some small holes were made on the crucible base and the top cover to allow a hydrogen flow through the samples, to remove the copper vapor that leaves the matrix during the physical decopperization process. Because of that, it was possible to remove more than 75% of copper mass from the samples bulk during the heating process, making easier the removal of the 25% of residual copper that remains commonly on the contact surfaces between the samples and the alumina disks put among them.

3.3. Microstructural characterization

Besides the copper removal, the physical decopperization has two other goals: the densification of the tungsten structure and the interconnection of pores. At the final step, uniform densification of around 7% was obtained. Besides the densification, an average of 34.9% of pores volume could be observed, in agreement with the results obtained in previous work with similar parameters[12]. The results, obtained by Archimedes' method for three reference samples, can be seen in Table 4. Optical micrographs obtained in a porosity analysis module to a decopperized sample can be seen in Figure 9. The numbers agree with Archimedes' method results.

Table 5 showed the EDX analysis results confirming the eutectic MoRu alloy composition. Before melting, the alloy composition changed due to the powder sedimentation in the brazing paste. However, after melting it was possible to observe the meniscus formation in the sample holder inner wall as well the MoRu eutectic alloy, as can be seen in Figure 10.

Optical micrographs taken to samples brazed at 1890°C and 1967°C can be seen in Figures 11a and 11b, respectively. The pictures indicate that there is no fillability by the alloy in temperatures below the alloy melting point (at 1955°C), which is notable in the sample brazed in a temperature above that.

Table 4. Apparent porosity calculated by the Archimedes' method.

Sample	Apparent porosity (± 0.5%)	Relative density (± 0,1 g/cm^3)	Bulk density (± 0,1 g/cm^3)
01	34.9	10.1	11.7
02	34.7	9.5	11.2
03	38.5	9.3	11.9

Table 5. EDX analysis of the Mo-Ru alloy surface before and after the melting process.

Element	Before (± 0.01 mol %)	After (± 0.01 mol %)
Mo	69.89	57.82
Ru	29.90	42.18
Others	< 0.21	-

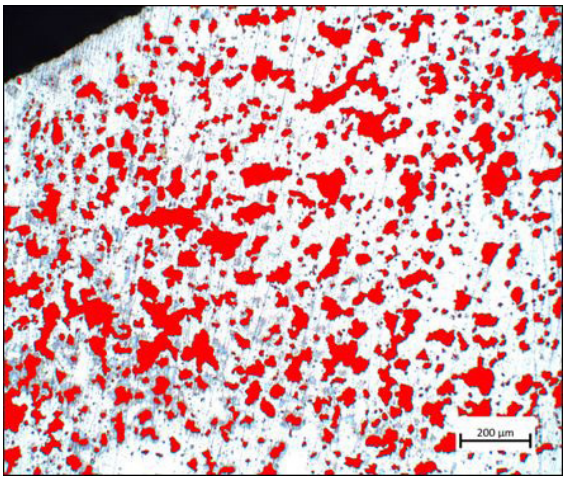

Figure 9. Optical micrograph of a decoppered sample taken with the microscope porosity analysis module.

The filling observed in the junction area and the absence of pores in the Mo-Ru system region indicates a melting phenomenon in that volume, which gives one some information about the junction's effectiveness. Moreover, it is noticed a seal produced on the bottom face of the cathode in Figure 11b. This is especially relevant to avoid back emission from the cathode button to the heater when the thermionic cathode is under operation.

SEM micrographs were then taken to check some atomic diffusion between the parts that could assure a chemical reaction between them to the Mo-Ru system. A picture of the sample taken with 150x magnification in the same region that Figure 11b was taken with SEM can be seen in Figure 12. It is possible to identify four different regions. On left, there is a dark gray color region related to the Mo body, region 1. At right, almost white color, there is the porous tungsten button, region 2. Between them, there is a gap of light gray color, related to Mo-Ru filler, region 3, and above, almost dark color, it is the Mo cathode body also.

The transition between regions 1 and 2 is easily noticed because of the difference of atomic mass between molybdenum and tungsten. On the other hand, the transition between regions

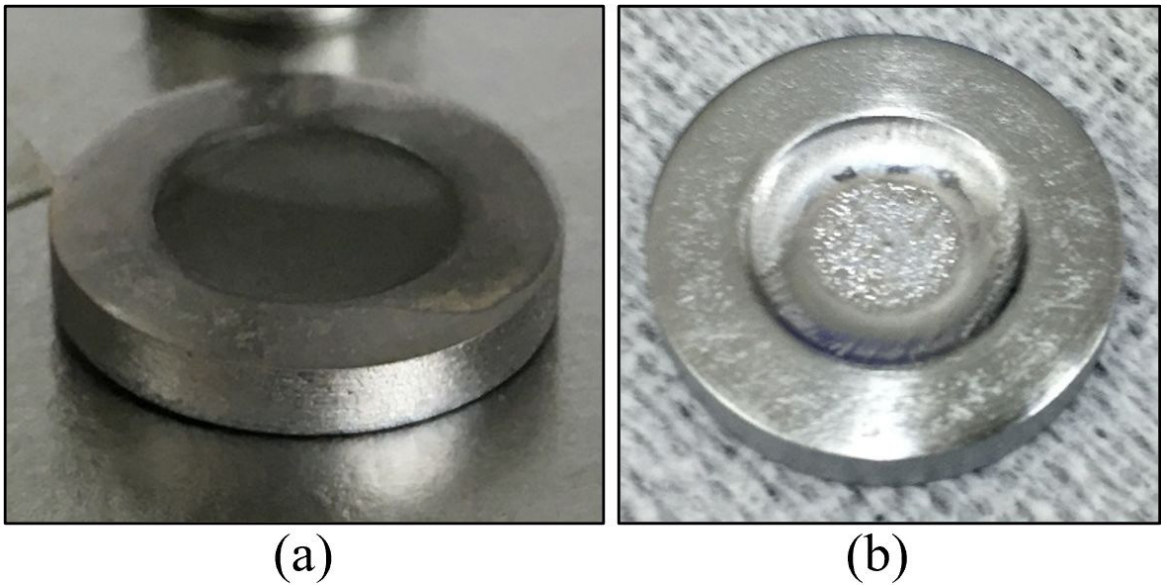

Figure 10. Sample prepared to analyze the melting of eutectic alloy of Mo-Ru system, (a) before melting (b) after melting.

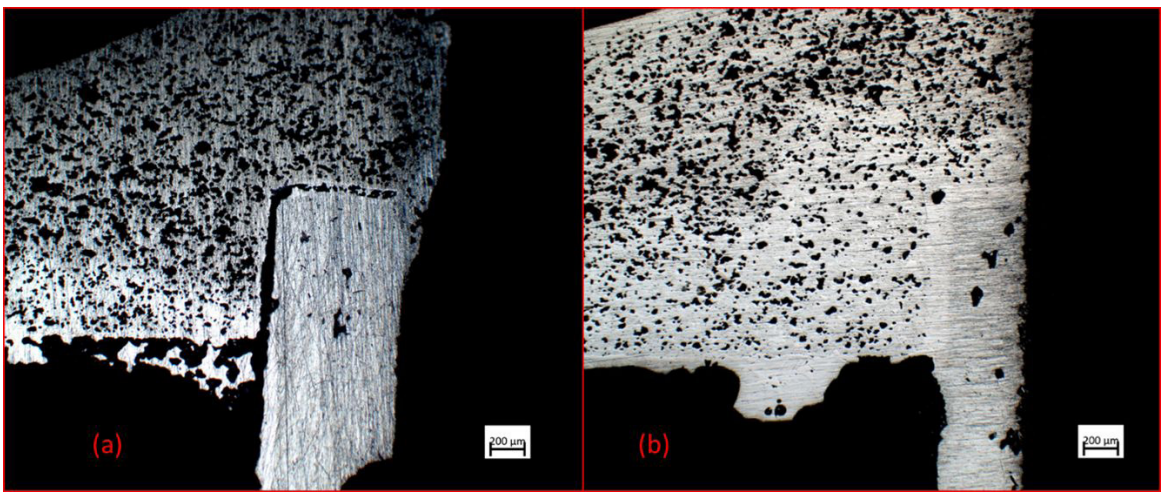

Figure 11. (a) optical micrograph of an 1890°C brazed sample, and (b) optical micrograph of a 1967°C brazed sample.

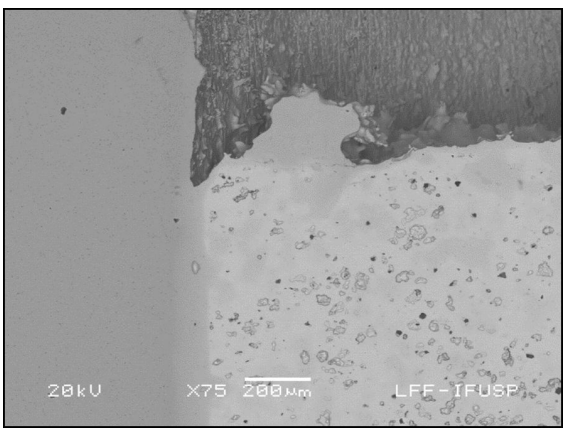

Figure 12. Scanning electron micrograph of a 1967°C brazed sample.

2 and 3 is quite diffused. It can be explained by the fact of the main specimen in both the regions being the same, and in the case of Mo-Ru system, the ruthenium atomic number is near to the molybdenum one, promoting almost no contrast when analyzed by backscattered electrons. In magnification above 800x SEM analysis, no difference can be noticed between these two regions, which is indicative evidence of a chemical reaction all along the junction, leaving no gap between them.

Additionally, an EDS map can be seen in Figure 13 considering the (a) junction, (b) molybdenum, (c) ruthenium, and (d) tungsten is shown. Figure 14 shows the full-scale counting spectrum and Table 6 shows the element percentage in that counting. It can be observed at the molybdenum map a more frequent counting in the cathode body region, at the tungsten map a more frequent counting in the matrix region and at

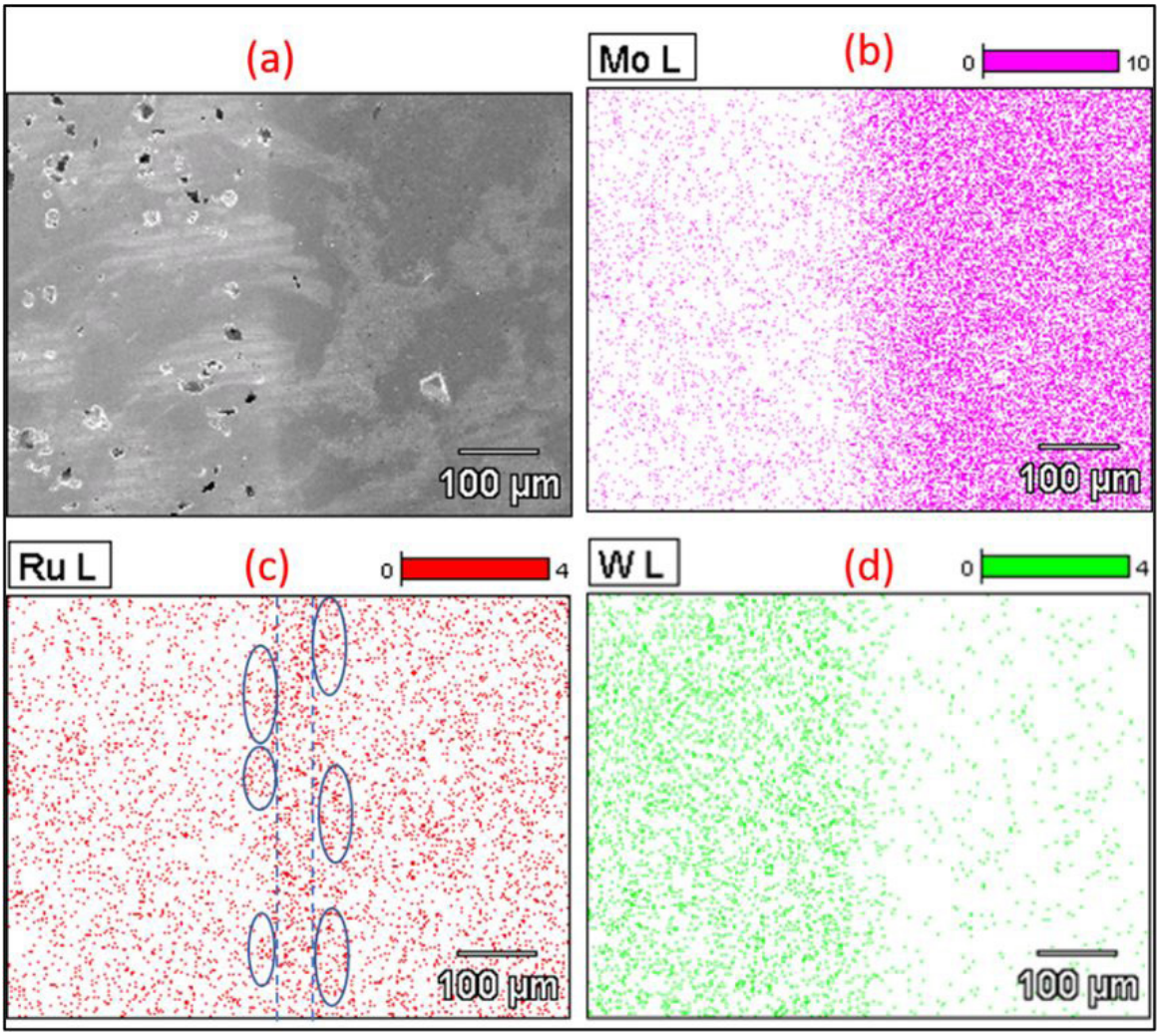

Figure 13. (a) SEM with a 150x magnification in the junction area, (b) EDS map counting Mo in the junction area, (c) EDS map counting Ru in the junction, and (d) EDS map counting W in the same region.

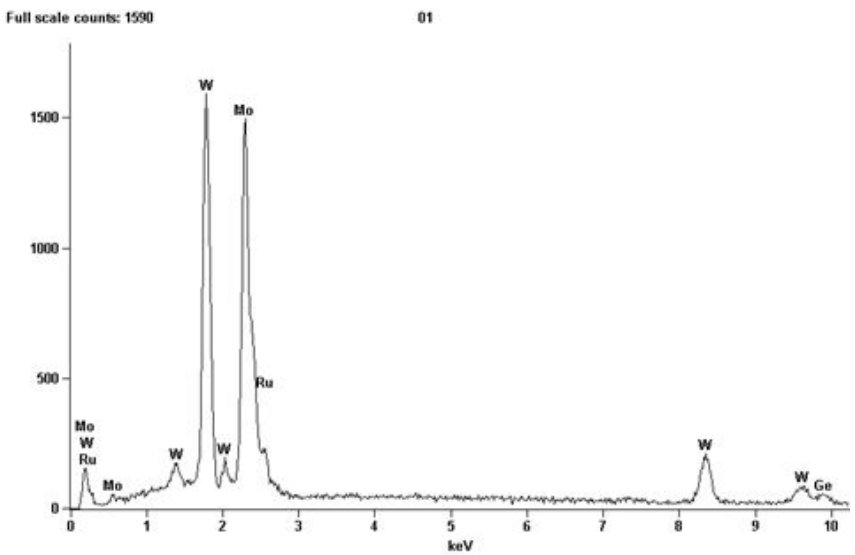

Figure 14. EDS full-scale counting spectrum taken in micrograph analysis in SEM micrograph with a 150x magnification in the junction area.

the ruthenium map a more frequent counting in Mo-Ru system region. As it is circled in Figure 13c there are some areas, in the brazed parts, where a ruthenium concentration is found. This result allows one to infer that there was an atomic diffusion of that specimen to the brazed parts.

3.4. Mechanical strength

As it was expected, the possible results of the stress-strain test were the brazing junction fracture, separating the parts (button and body), a body rupture, which could not be qualifying specifically the junction characteristic rupture tensile, and the button fracture that would have the same effect.

Making a direct calculus considering the bottom punch area and the applied load in the test, we obtained the pressure that promoted the sample fracture. The values obtained were from 62 to 250 MPa, as it can be seen in Table 7. The fracture in the samples tested was observed at the porous matrix and the cathode body, but none of them were observed at the brazing area. The result can be seen in Figure 15. Furthermore, it could be observed that a wide range of fracture loads was obtained, besides that, the samples cracked at different regions and different geometrical characteristics were observed on the cracks.

In SEM image expressed in Figure 16a, an eccentric origin of crack propagation was observed, and the major cracks have a radial tracing, converging to the same region.

Table 6. SEM quantitative EDS specimens results.

Element	Weight %	Weight % Error	Norm. Wt % Err	Norm. Wt. % Err	Atom %	Atom % Error
Ge	0.97	+/- 0.83	0.97	+/- 0.83	1.62	+/- 1.39
Mo	49.99	+/- 0.85	49.99	+/- 0.85	62.95	+/- 1.07
Ru	5.96	+/- 0.52	5.96	+/- 0.52	7.12	+/- 0.62
W	43.08	+/- 2.24	43.08	+/- 2.24	28.31	+/- 1.47
Total	100.00		100.00		100.00	

Figure 15. (a) cathode sample 1 after strength test, and (b) cathode sample 3 after strength test.

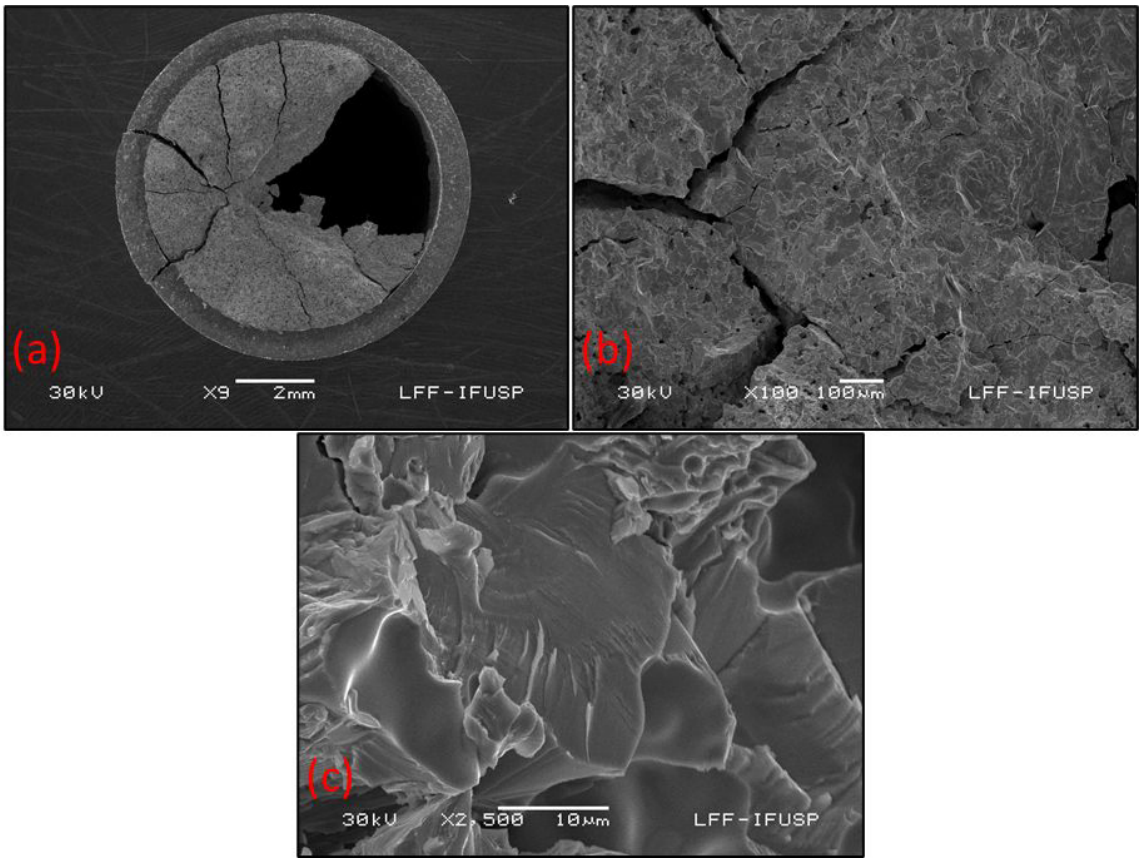

Figure 16. SEM fractography of brazed cathode in the (a) overview surface, (b) cracks propagation origin region and (c) grains brittle fracture.

Table 7. Strength test results from 5 cathode samples brazed at 1967°C.

Sample	Fracture stress (±1 MPa)	Fracture point observed
1	62	porous matrix
2	78	porous matrix
3	195	cathode body
4	117	porous matrix
5	256	cathode body
Average	142	

This behavior was common in all the button cracked samples. Besides that, in higher magnification in the same area, as shown in Figures 16b and 16c, the rupture region gives us the information of a brittle fracture with an intergranular crack propagation, and some cleaved grains could be observed corroborating this hypothesis.

The observed variation in rupture tensile is highly probable to be caused by the internal tensions resulted of the lathe machine process in both, cathode body and cathode button. The fact of the cracks origin region not being in the center of the sample, where the tensile was directly applied, agrees with the previous hypothesis.

These qualitative results do not qualify specifically the brazing junction, but it gives some information that, in case of subjected to a mechanical strength, the alloy can sustain a higher applied load level than the parts. Despite these values being lower than typical values for metals that were found between 500 MPa and 800 MPa in similar works, the fragile structure and dimensions of cathode must also be considered. Besides that, this tensile strength is higher than that obtained in Ni-Mo system tests, 87.9 ± 0.5 MPa[9]. Considering that the stress work condition of the cathode is lower than the tensile strength for the tested samples, it can be inferred that the Mo-Ru system is a suitable option for this application.

4. Conclusion

The results related to copper removing and graphite contamination elimination are relevant improvements obtained by the physical decoppering arrangement using the molybdenum crucible under established parameters. The EDX analysis results showed process reproducibility.

At the final step, an average of 34.9% of pores volume was obtained by the Archimedes' method. This volume of pores is needed once a volume is necessary to be impregnated by the emission material in further steps. In addition, the results agree with previous works where over 20,000 h thermionic cathodes were obtained.

Considering the Mo-Ru as a brazing alloy in its eutectic composition the microscope analysis results indicated a complete gap filling as confirmed by the atomic diffusion

obtained by EDS in SEM analysis. The mechanical strength analysis showed that a brazing junction has higher tensile strength than the cathode parts. The porosity of the brazed cathode sample influenced the crack propagation, appearing to be the easiest path, providing a brittle fracture. Some grains in the micrograph showed cleaved rupture as a characteristic of the same failure behavior.

Based on the contamination-free matrix manufactured results, and the mechanical and thermal stable formed junction obtained by using the chosen brazing system, it can be concluded that the metallurgical process developed could be considered as an appropriate option for impregnated thermionic cathodes manufacture.

5. Acknowledgments

The authors would like to thank BNDES (contract number 14.2.0784.1) for the financial support.

6. References

1. Umstattd RJ. Advanced electron-beam sources. In: Barker RJ, Luhmann NC, Booske JH, Nusinovich GS, editors. Modern microwave and millimeter-wave power electronics. New Jersey: Wiley-IEEE Press; 2005. Chapter 8.
2. Barker RJ, Schamiloglu E. High-power microwave sources and technologies. New Jersey: Wiley-IEEE Press; 2001. Chapter 9, Cathodes and electron guns.
3. Gilmour AS. Principles of traveling wave tubes. Norwood, MA: Artech House; 1994. Chapter 5.
4. Cronin JL. Modern dispenser cathodes. IEE Proc. 1981;128:19-32.
5. Shroff AM. Review of dispenser cathode. Rev Tech Thomson – CSF. 1991;23:958-65.
6. Higashi C, Lima NB, Matos JR, Giovedi C, Motta CC. Investigation of electron emitting barium-calcium aluminate fabrication process for impregnated microwave tube cathodes. In: 2005 SBMO/IEEE MTT-S International Microwave and Optoelectronics Conference; 2005; Brasília, Brazil. Proceedings. New York: IEEE; 2005. http://dx.doi.org/10.1109/IMOC.2005.1579982.
7. Schwartz MM. Brazing. 2th ed. Ohio: ASM International; 2003. Chapter 2.
8. Roberts P. Industrial brazing practice. 2th ed. New York: CRC Press; 2013. p. 11-8.
9. Sene FF, Motta CC. Synthesis and characterization of Ni-Mo filler brazing alloy for Mo-W joining for microwave tube technology. Mater Res. 2013;16(2):417-23. https://doi.org/10.1590/S1516-14392013005000019.
10. Hiraoka Y. High-temperature annealing embrittlement of single-crystalline molybdenum joined by using Mo-40% Ru alloy. Refract Met Hard Mater. 1992;11(2):89-95.
11. Infomet. Binary Mo-Ru diagram [Internet]. 2020 [cited 2020 Dec 30]. Available from: https://www.infomet.com.br/site/diagrama-de-fases-ver.php?cod=321.
12. Sene FF, Silva AGL, Motta CC. Development and characterization of the porous tungsten matrix obtaining process for dispenser thermionic cathode. In: Vacuum Electron Sources Conference (IVESC); 2012; Monterey, CA, USA. New York: IEEE; 2012. p. 1-2. http://dx.doi.org/10.1109/IVESC.2012.6264175.
13. Costa FA, Silva AGP, Ambrozio F Fo, Gomes UU. Solid state sintering of a W-25w% Ag powder prepared by high energy milling. Int J Refract Met Hard Mater. 2008;26(4):318-23.
14. ASTM: American Society for Testing and Materials. Standard test methods for apparent porosity, water absorption, apparent specific gravity, and bulk density of burned refractory brick and shapes by boiling water [Internet]. West Conshohocken: ASTM; 2021 [cited 2021 Jan 17]. Available from: https://www.astm.org/Standards/C20.htm.